Since January 2020 Elsevier has created a COVID-19 resource centre with free information in English and Mandarin on the novel coronavirus COVID-19. The COVID-19 resource centre is hosted on Elsevier Connect, the company's public news and information website.

International Journal of Biological Macromolecules 220 (2022) 1415–1428

Contents lists available at ScienceDirect

International Journal of Biological Macromolecules

journal homepage: www.elsevier.com/locate/ijbiomac

Exploring the anti-SARS-CoV-2 main protease potential of FDA approved marine drugs using integrated machine learning templates as predictive tools

Naila Attiq [a], Uzma Arshad [a], Simone Brogi [b], Nusrat Shafiq [a,*], Fazeelat Imtiaz [c], Shagufta Parveen [a], Maryam Rashid [a], Nadia Noor [d]

[a] Synthetic and Natural Products Discovery (SNPD) Laboratory, Department of Chemistry, Government College Women University Faisalabad, 38000, Pakistan
[b] Department of Pharmacy, University of Pisa, Via Bonanno 6, 56126 Pisa, Italy
[c] Green Chemistry Laboratory, Department of Chemistry, Government College Women University Faisalabad, 38000, Pakistan
[d] Micro-biology Laboratory, Department of Chemistry, Government College Women University Faisalabad, 38000, Pakistan

ARTICLE INFO

Keywords:
Activity atlas model
Activity cliff
Holichondrin B
Field template
Marine drugs
COVID-19

ABSTRACT

Since the inception of COVID-19 pandemic in December 2019, socio-economic crisis begins to rise globally and SARS-CoV-2 was responsible for this outbreak. With this outbreak, currently, world is in need of effective and safe eradication of COVID-19. Hence, in this study anti-SAR-Co-2 potential of FDA approved marine drugs (Biological macromolecules) data set is explored computationally using machine learning algorithm of Flare by Cresset Group, Field template, 3D-QSAR and activity Atlas model was generated against FDA approved M-pro SARS-CoV-2 repurposed drugs including Nafamostat, Hydroxyprogesterone caporate, and Camostat mesylate. Data sets were categorized into active and inactive molecules on the basis of their structural and biological resemblance with repurposed COVID-19 drugs. Then these active compounds were docked against the five different M-pro proteins co-crystal structures. Highest LF VS score of Holichondrin B against all main protease co-crystal structures ranked it as lead drug. Finally, this new technique of drug repurposing remained efficient to explore the anti-SARS-CoV-2 potential of FDA approved marine drugs.

1. Introduction

In December 2019 the world health organization (WHO) named infectious disease as coronavirus that caused by newly revealed coronavirus [1,2]. The world health organization (WHO) declared covid-19 as epidemic disease in March 2020 due to its wide spread infectivity and high contagious rate [3,4]. ICTV (the International Committee on Taxonomy of Viruses) on Feb 11, 2020 retitled this corona infection as the severe acute respiratory syndrome coronavirus 2 [5,6]. Covid-19 epidemic initiated by the SARS-CoV-2 (severe acute respiratory syndrome coronavirus 2) [4,7]. According to the analysis of phylogenetic the virus responsible of severe acute respiratory syndrome coronavirus 2 has great resemblance to earlier coronavirus MERS-CoV and SARS-CoV-1 [7–9]. In Wuhan China new SARS-CjoV-2 virus was first detected [10]. The first fifty days of epidemic killed more than 1800 individually and seventy thousand people were infected by this virus. On 5th April 2021 the virus statistics exhibit almost 245,321,425 confirmed coronavirus cases and in 220 countries 4,979,605 deaths were announced [11,12] https://www.worldometers.info/coronavirus/. Coronavirus disease is extremely infectious and its main symptoms are headache, fever, dry cough, dyspnea, sore throat, gastrointestinal issue and myalgia [3]. In some cases, severe patient gone through ARDS (acute respiratory distress syndrome) that lead towards expiry [5,13]. The Infection rate and the transmission potency of covid-19 is so fast [14]. Due to high transmission rate of the epidemic Covid-19 is outbreak all around the world [15]. Coronavirus is enclosed solitary stranded RNA viruses with a helical symmetry of nucleocapsid [10,16]. Coronavirus belong to the coronaviridea family of beta genus [17]. It has a sphere-shaped envelope. The envelope of Covid-19 has spike-like glycoprotein projections [18]. Several corona infections also comprise a HE (hem agglutinin-esterase) protein [19]. The genome of coronaviruses encrypts some sps (structural proteins) and nsps (nonstructural proteins) [18,20]. The sps are accountable for host contagion, virus assembly, fusion of membrane, and morphogenesis [20,21]. Also particles of virus released

* Corresponding author.
E-mail addresses: simone.brogi@unipi.it (S. Brogi), dr.nusratshafiq@gcwuf.edu.pk (N. Shafiq).

https://doi.org/10.1016/j.ijbiomac.2022.09.086
Received 21 July 2022; Received in revised form 9 September 2022; Accepted 9 September 2022
Available online 16 September 2022

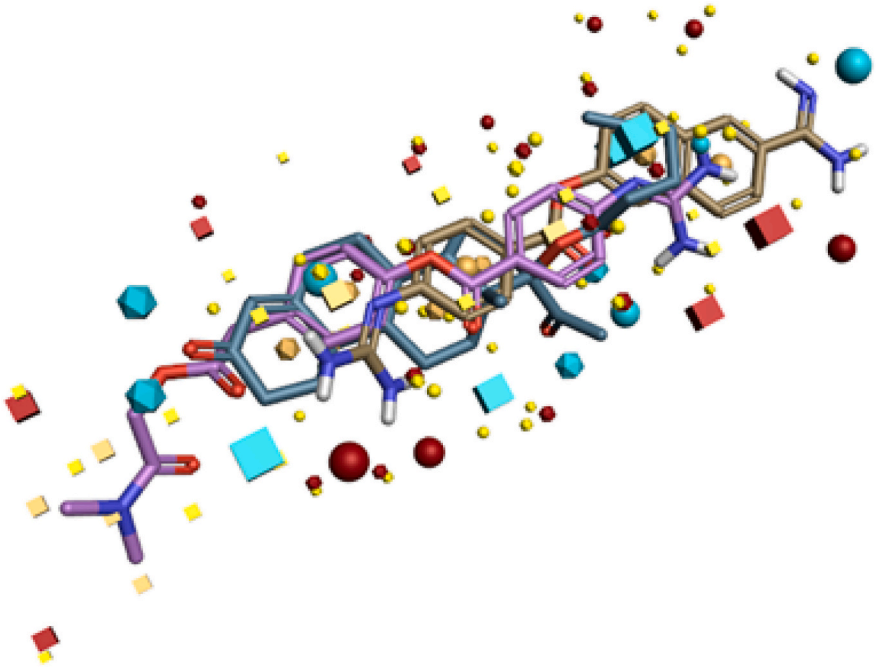

Fig. 1. Pharmacophore field points generation of SARS-CoV-2 FDA approved drugs from field template tool of Flare.

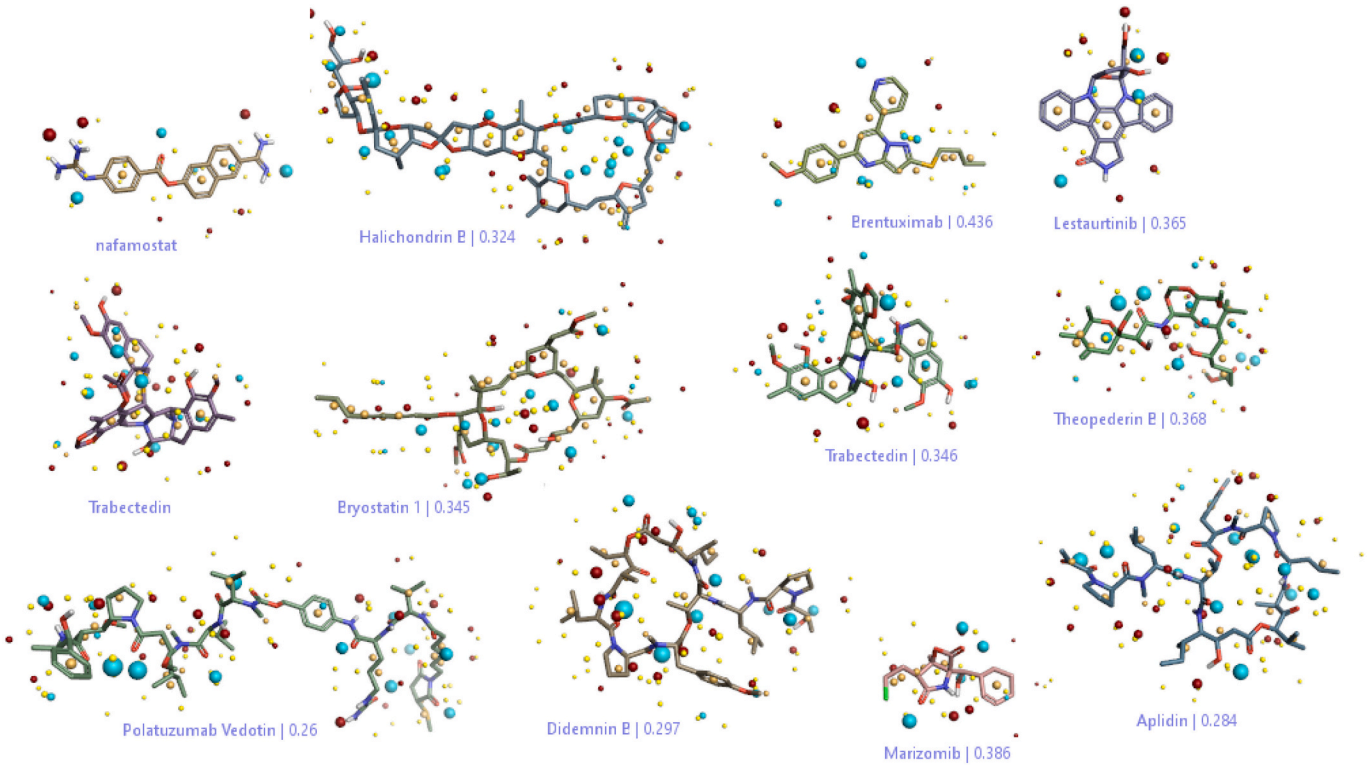

Fig. 2. Field Points of marine active compounds generated from FDA approved SARS-CoV-2 repurposed drug.

between other functions due to structural proteins. The nsps (nonstructural proteins) enable virus transcription and replication [18,22]. The spike (S), membrane(M) and envelope (E) genes encrypt the sps (structural proteins) [23]. The severe acute SARS-CoV-2 enters into human cells through spike protein by interact with the angiotensin-converting enzyme 2 (ACE2) [24–26].

Covid-19 is polypeptide that is cleaved by alter protease viz. chymotrypsin like protease and papain like protease that foremost to the establishment of some nsps (nonstructural proteins) that are essential for virus-related replication [27,28].

The replicas genetic factor of SARS-CoV-2 encodes with two overlapping polyproteins—pp1a and pp1ab—that are mandatory for viral transcription and replication [7].

Through an extensive proteolytic process, the functional polypeptides are released from these two polyproteins (pp1a and pp1ab) [29]. SARS-COV-2 is +ssRNA virus that encrypts several nonstructural

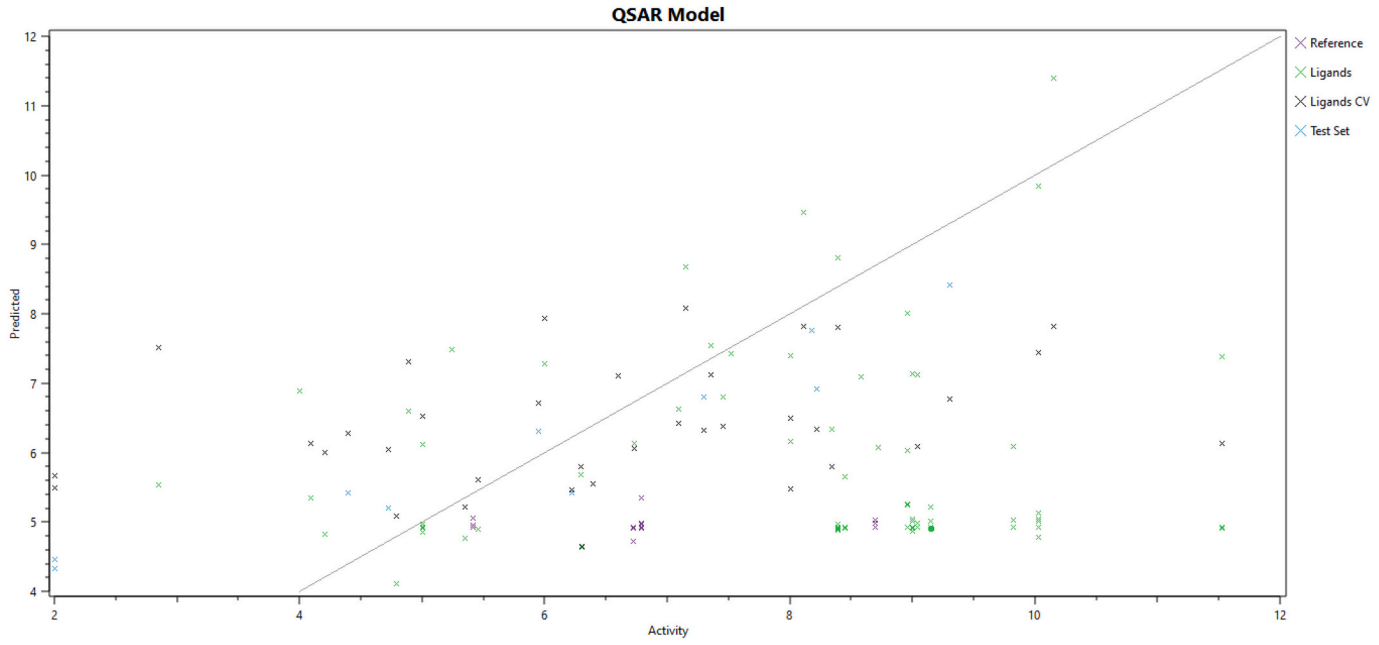

Fig. 3. Fitness plot representing Ligands as Training set, Ligands cross validated (CV) as LOOCV, Test set and Reference generated from 32 training set ligands and 17 test set ligands.

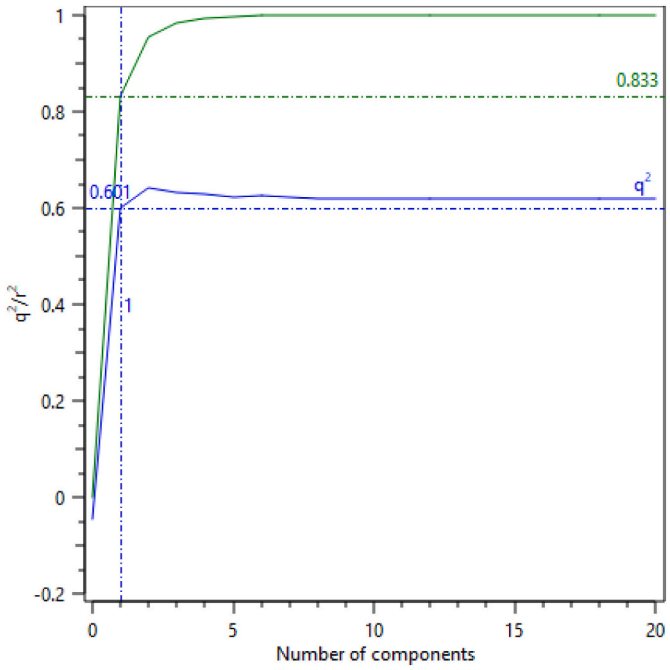

Fig. 4. 3D-QSAR graph showing the fitness of model by plotting cross validated regression co-efficient (q^2) blue color along with regression co-efficient (r^2) green color against number of components of model. (For interpretation of the references to color in this figure legend, the reader is referred to the web version of this article.)

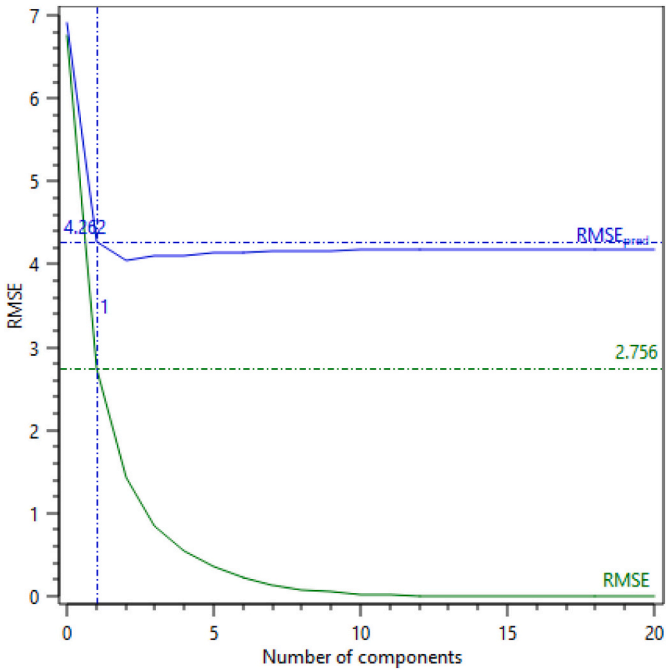

Fig. 5. 3D-QSAR model graph showing predicted root mean square error (blue color) versus experimental root mean square error (green color). (For interpretation of the references to color in this figure legend, the reader is referred to the web version of this article.)

and structural proteins [30]. Main protease (M pro) is nonstructural protein and also known as 3-chymotrypsin-like protease (3CLpro) [31]. M pro is accountable for the eleven main maturation cleavage sites and also foremost for the establishment of NSPs [24]. For the treatment of SARS-COV-2 non-structural proteins may have greater potential to be target site for the antiviral drugs [31]. In SARS-CoV-2 all active sites located on main protease. The coronavirus M pro is 3 domain cysteine protease, Domains I and II have an antiparallel β-barrel structure. Domain III contain globular cluster of five helices [30–32] which features a Cys145-His41 catalytic dyad located in the cleft between domains I and II [33,34]. Domain III is liable for the dimerization of enzyme [32].

In the viral life cycle many upstream replicative events of SARS-CoV Mpro process in polyprotein that involved in indispensable. Mpro had effect on lowering progeny virus it also enhances the cell survival and

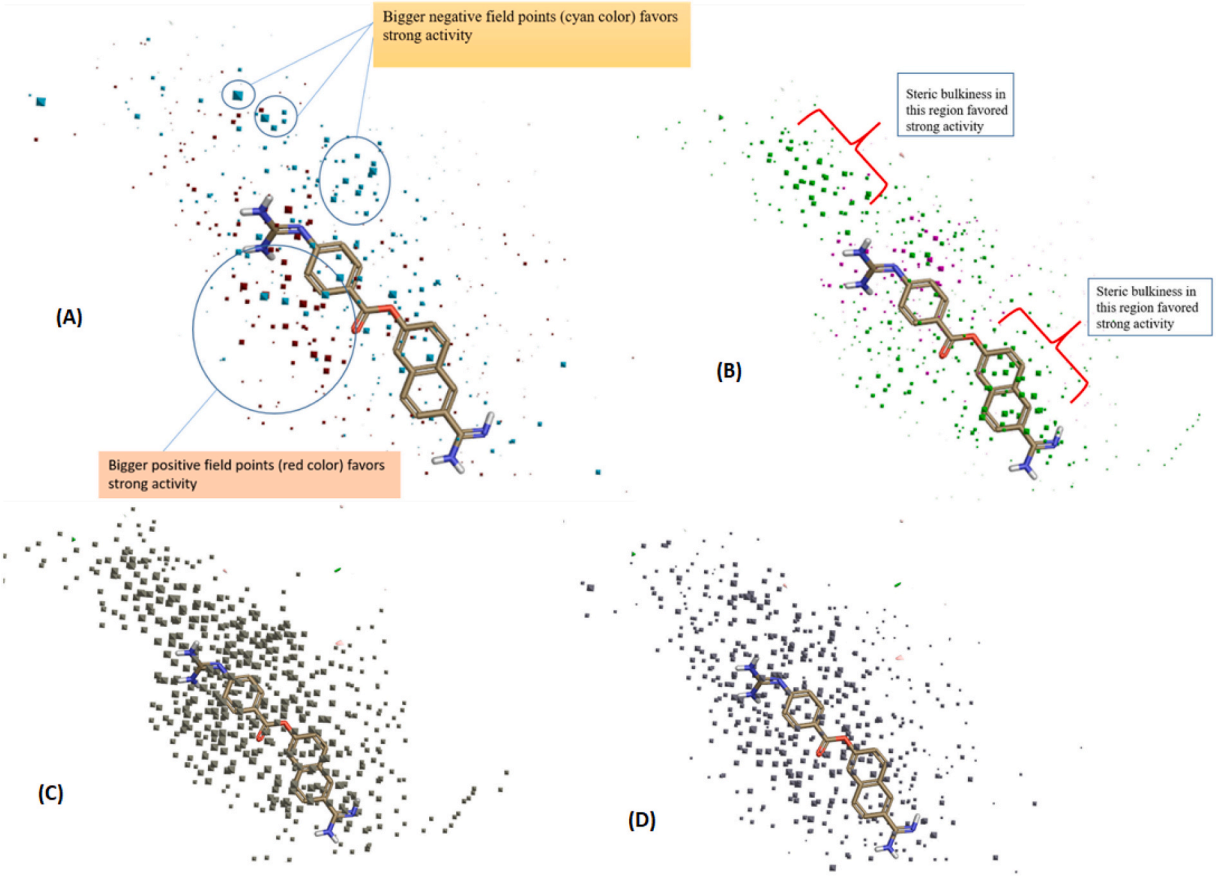

Fig. 6. 3D view of QSAR model using reference compound Nafamostat depicting the high/low biological activity areas in molecules (A) Model field points in cyan color (negative electrostatics) and red color co-efficient field points (positive electrostatics) showing the stronger activity areas. (B) Steric bulkiness model, representing green color region contributing for high biological activity, purple color representing the unfavorable contribution of steric character towards biological activity enhancement. (C) Steric Variance (D) Electrostatic Variance, both variances have points with regions of high changes and low changes. (For interpretation of the references to color in this figure legend, the reader is referred to the web version of this article.)

reduce peptide's function. Thus small molecule-mediated blocking of Mpro activity is a feasible option for SARS-CoV-2 anti-viral drug development [31,34].

Conventional drug development and drug discovery has not kept up with challenges from evolving diseases like MERS-CoV, Ebola virus and currently SARS-CoV-2. Along with this, over extravagant costs, high consumption rate and long market approval time periods are the major delaying factors in new drug designing process. Accompanying these reasons, drug developers and medicinal chemists consider drug repositioning or repurposing an effective, time saving and an efficacious strategy in comparison to de novo drug designing. Main advantage of this technique is that pharmacological properties and toxicity factors are already in knowledge [35].

About 75 % earth composite of water but there was not enough research have carried out on the marine organism pharmacology and literature showed a limited work on their pharmaceutical effects. If observe, marine sources have diverse collection of new drugs against major dieses like cancer, malaria, microbial infections [36]. Ocean is an exceptional and diverse source of bioactive pharmaceutical natural metabolites with structural, chemical and biological diversity than terrestrial natural products [11]. Marine source provide a great opportunity for discovering and introducing about 13,000 natural products with diseases curative properties [37,38]. Marine natural metabolites are designed as major pharmacophore. According to a literature based survey, about 68 % of FDA approved drugs concise of marine to cure infectious disease and 63 % as anti-cancer drugs [39,40]. Marine sources play a vital role in emergence of drug development during 20th century by isolation of penicillin, streptomycin, vincristine that extend life span by improving the quality of life. With the advancement of techniques and research development, there has observed a change in industrialization to become more sophisticated to discover drug and programs initiated to design drug based on a biochemical target [41].

In this study, FDA approved marine drugs were selected as repurposed drug for combating SARS-CoV-2 owing to their structural diversity, high efficacy in controlling disease with potential IC_{50} values. COVID-19 main-protease was targeted in this paper and for this purpose computer aided drug designing (CADD) techniques were employed. Machine learning algorithm of Flare by Cresset group was employed comprising field template, activity atlas and molecular docking. Promising results for FDA approved marine drugs were obtained after employing CADD techniques [7].

2. Materials and methods

2.1. Standard parameters for field point generation, 3D-QSAR and activity atlas model development

2.1.1. Retrieval of compounds for data set preparation

Dataset preparation of 49 marine drugs was carried out by collecting FDA approved marine drugs from prior literature containing research papers and reports. Moreover, many marine drugs were assembled from different repository of compounds like [42,43]. Compounds acquired from literature were sketched into 2D-chemical structure using ChemDraw 20.1.1, then converted into SDF module using Chem3D 20.1.1.

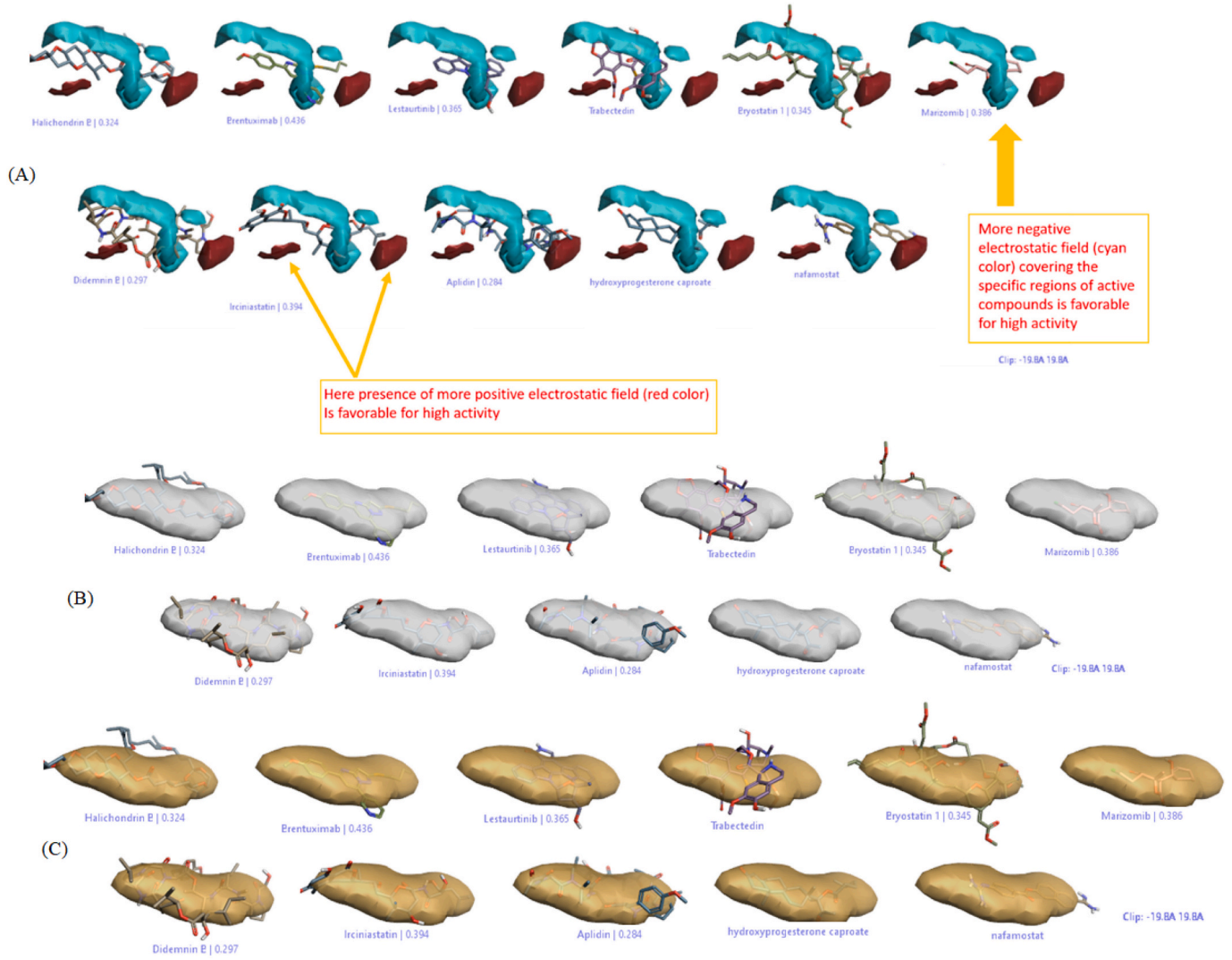

Fig. 7. SAR model of active compounds derived from activity atlas analysis of marine dataset. (A) Positive electrostatic region shown in red color and negative electrostatic region shown in cyan color revealing the favorable and unfavorable regions for biological activity enhancement, (B) Active molecules revealing average shape (white shape), (C) Hydrophobic interactions (yellow color) regions of active molecules. (For interpretation of the references to color in this figure legend, the reader is referred to the web version of this article.)

Table 1
Activity score of active compounds obtained after activity atlas average model.

Sr. no.	Structure	"Average of actives" model activity pIC_{50} values
1	Bryostatin	8.39
2	Halichondrin B	10.03
3	Aplidin	9.00
4	Marizomib	8.45
5	Trabectedin	9.82
6	Bretuximab	11.52
7	Didemnin B	8.96
8	Lestaurtinib	9.04

While compounds fetched from online repositories were save into SDF format directly. pH of molecules is assumed to 7.0 by using Flare Software (Cresset Inc., UK) protonation state module. The biological potential of these molecules was expressed in minimum inhibitory concentration (IC_{50}) and transformed to positive logarithm values by using the formula $pIC_{50} = -\log(IC_{50})$ [44–46].

2.1.2. Field point generation

Marine drug dataset was loaded to flare along with three (3) reference (standard) drugs used in COVID-19 treatment named as Nafamostat, Hydroxyprogesterone caporate, and Camostat mesylate. For pharmacophore generation field points/templates were added to these four COVID-19 repurposed drugs, in order to use these drugs as bioactive conformations [47,48]. Fig. 1 displays the field points template features of SARS-CoV-2 repurposed drugs by using Forge visualization tool. As these field points generate the four diversified molecular fields containing positive and negative electrostatic potential surface, shape and hydrophobic field surface [49–51].

2.1.3. Confirmation hunt and alignment

All the molecules in marine database were set to Accurate but Slow Conformation Hunt. Conformations Hunt of dataset were generated by adding 90 field points from reference drugs conformation and maximum number of conformations generated for each molecule was set to 200. RMSD cut off value for duplicate conformers was 0.5 Å and cutoff gradient was 0.100 kcal/mol for conformer minimization. Energy window for hunt was set to 3 kcal/mol. Alignment of molecules was generated from three (3) reference drugs, normal alignment was carried out using Maximum Common Substructure (MCS) along with default thresholds settings.

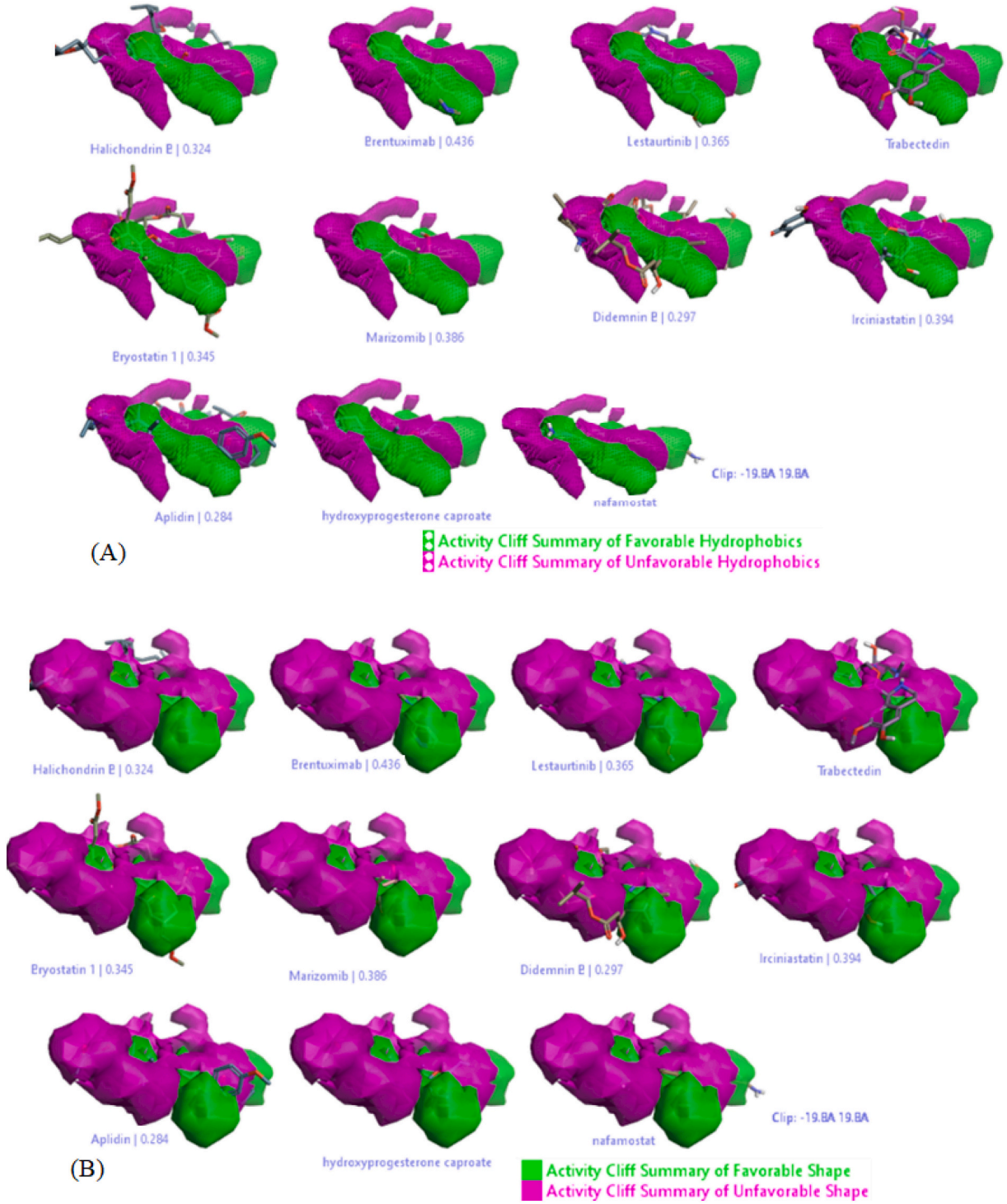

Fig. 8. SAR mechanism activity cliff summary models of active compounds, (A) Favorable Hydrophobics (green color) and unfavorable hyrophobics (magenta) (B) Green color showing favorable shape and magenta color showing unfavorable shape. (For interpretation of the references to color in this figure legend, the reader is referred to the web version of this article.)

2.1.4. 3D-QSAR and activity atlas model development

For 3D-QSAR model building, marine data set was divided into 80 % training set molecules and 20 % test set molecules. A normal Field based QSAR model was generated by selecting the pIC_{50} values as partition method. Maximum number of components was set onto 20, minimum distance for sample point was fixed to 1.0 Å, and electrostatic fields were used in model building. 3D-QSAR model was built using Partial Least Square (PLS) regression analysis [44,52].

2.1.5. Validation of field QSAR using statistical parameters

Field QSAR model was validated by regression co-efficient (R^2) and cross-regression co-efficient (q^2) of training and test set molecules. Leave-one-out (LOO) technique was used to optimize the molecules for QSAR model building. This method is effective for models containing small number of training data set.

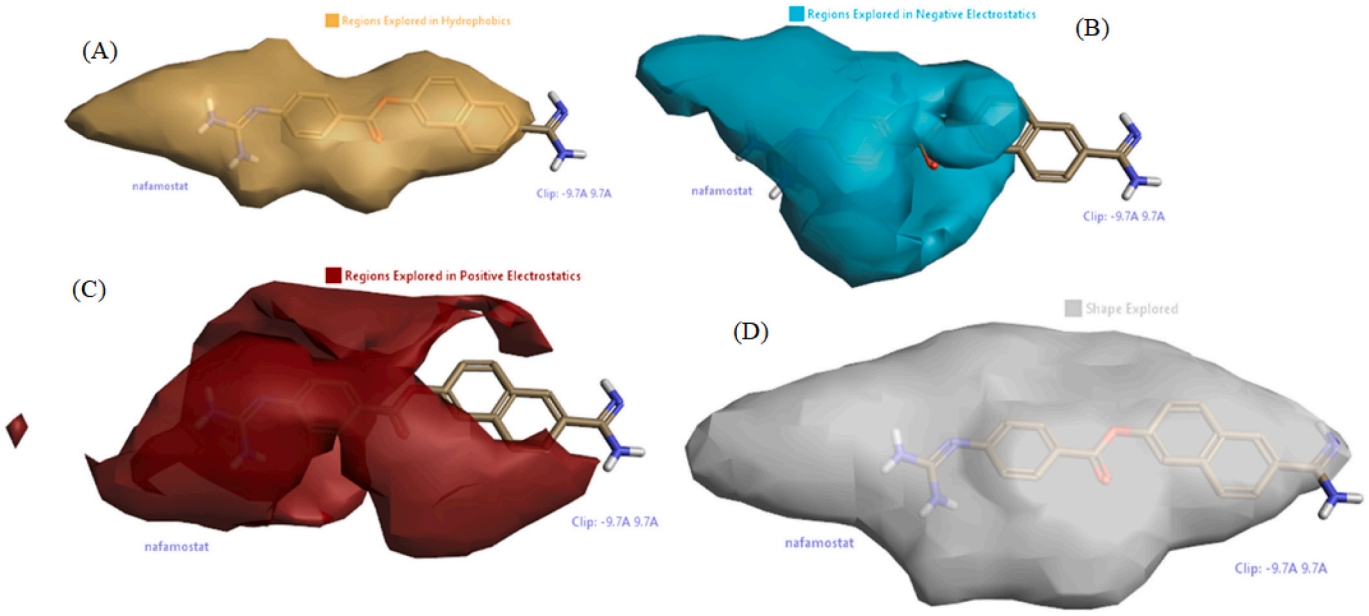

Fig. 9. Regions explored by active molecules in activity atlas model visualized by reference molecule Nafamostat, (A) Regions explored in Hydrophobic (B) Regions explored in negative electrostatics (C) Regions explored in positive electrostatics (D) Regions explored in average active shape.

2.1.6. Activity atlas model for visualization of SAR

Activity atlas model provide the structural insight for understanding of the structure activity relationship (SAR) of library of compounds. To construct activity atlas model utilizing marine database an average of active compounds, activity cliff summary models and electro-potential regions explored were generated against four FDA approved SARS-COVID-19 repurposed drugs as reference. Activity-Atlas QSAR Model was built using pIC_{50} field. These biochemical computed activity models explored the active regions and active compounds from marine data set. From activity Cliff model smoothing radius for structural similarity between active compounds of marine database and SAR-CoV-2 FDA approved drugs came out to be 40 % [52,53].

2.2. Molecular docking simulations

2.2.1. Protein preparation

The co-crystallized structures of five COVID-19 main protease in complex with different reference ligands was downloaded using Protein interface of Flare GUI from RSCB Protein Data Bank (PDB), having (PDB ID: 7BUY, 7CA8, 7JQ2, 7L0D and 7BQY) respectively. Full protein preparation was applied on the 3D co-crystal target receptors using protonation state module by setting all the protein preparation parameters i.e., grid preparation, pH to 7.0, active site size to 6.00 Å and adding ligand role as reference. Heteroatoms and water molecules were removed and hydrogen atoms were added along with missing atoms [54].

2.2.2. Normal molecular-docking simulation parameters

For docking of molecules, Normal Docking tool was used present in Flare software. For this screening pool and population size was set to 1, with one (1) run and ten (10) maximum numbers of poses. All the ligands were minimized before docking. For best pose prediction Flare software uses Lead Finder. The binding free energy algorithm predict the excellent pose and best binding affinity was predicted by Virtual Screening score. Types of interaction between protein and ligand were also provided by Lead Finder comprising H-bonding, Pi and alkyl interactions and Van der Waals forces [7,55].

2.3. Molecular dynamics simulations

Molecular dynamics (MD) studies were conducted using Desmond 5.6 academic version via Maestro (Desmond Molecular Dynamics System, version 5.6, D. E. Shaw Research, New York, NY, 2018. Maestro-Desmond Interoperability Tools, Schrödinger, New York, NY, 2018). MD simulations were accomplished on two NVIDIA GPUs, employing the Compute Unified Device Architecture (CUDA) API. The complexes resulting from molecular docking studies were inserted into an orthorhombic box together with water molecules (solvent model TIP3P) using Desmond system builder available in Maestro. MD simulations were executed employing the force field OPLS. Na^+ and Cl^- ions (0.15 M) were added to mimic the physiological concentration of monovalent ions. The ensemble class NPT (constant number of particles, pressure, and temperature) were utilized employing a constant temperature of 310 K and a pressure of 1.01325 bar. To integrate the equations of motion, RESPA integrator was applied. Nose-Hoover thermostats and the Martyna-Tobias-Klein method were used for keeping constant temperature and pressure of the simulation, respectively. Particle-mesh Ewald technique (PME) was used to calculate the long-range electrostatic interactions. 9.0 Å was selected as the threshold for the van der Waals and short-range electrostatic interactions. The systems were equilibrated using the default procedure, which consists of a series of restrained minimization and MD simulations to gradually relax the system. As a result, a single 100 ns trajectory was determined for each complex. MD simulation studies were independently repeated two times for providing a more reliable output. Simulation Event Analysis tools, available in the software package, were used to examine the trajectory files. All charts relating to MD simulation presented in this article were created using the same tools. Therefore, the root mean square deviation (RMSD) was evaluated using the following equation:

$$RMSD_x = \sqrt{\frac{1}{N}\sum_{i=1}^{N} r'_i t_x - r_i t_{ref} 2}$$

$RMSD_x$; calculation for a frame x; N: number of selected atoms; t_{ref}: reference time, (normally the first frame is utilized as the reference at time $t = 0$); r': position of chosen atoms in frame x at time t_x, after the superimposition with the reference frame. Every frame in the simulation trajectory is subjected to the same technique. The following formula was

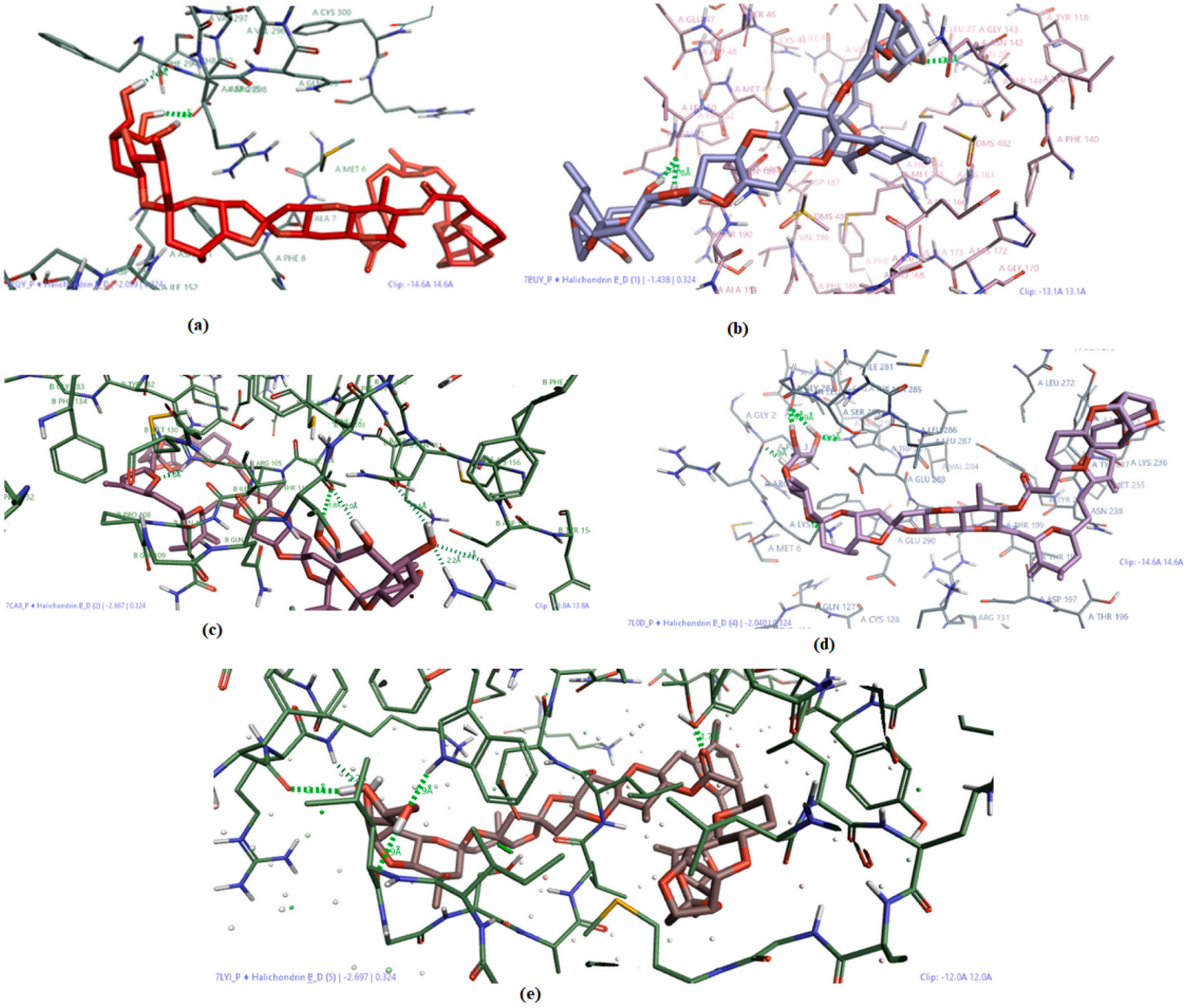

Fig. 10. Docked view of Lead Compound Holichondrin B with co-crystal protein structure of SARS-CoV-2 obtained after Ligand and Structural based drug designing (A) Docked Holichondrin B (red color) with COVID-19 main protease in complex with inhibitor N3 (PDB ID: 7BQY) (B) Docked Holichondrin B (blue color) with COVID-19 main protease in complex with Carmofur (PDB ID: 7BUY) (C) Docked Holichondrin B (violet color) with COVID-19 main protease in complex with Shikonin (PDB ID: 7CA8) (D) Docked Holichondrin B (light purple color) with COVID-19 main protease in complex with ML188 (PDB ID: 7L0D) (E) Docked Holichondrin B (brown color) with South African SARS-CoV-2 spike protein (PDB ID: 7LYP). (For interpretation of the references to color in this figure legend, the reader is referred to the web version of this article.)

used to calculate the root mean square fluctuation (RMSF):

$$RMSF_i = \sqrt{\frac{1}{T}\sum_{t=1}^{T} < r'_i t - r_i t_{ref} 2 >}$$

$RMSF_i$: generic residue; T: trajectory time considered for the calculation of RMSF, t_{ref}: reference time, r_i: position of residue i; r': position of atoms in residue i after superposition on the reference. The square distance is averaged over the atoms in the residue, as indicated by the angle brackets.

3. Results and discussions

3.1. Ligand based virtual screening

3.1.1. Pharmacophore model

For inhibiting the COVID-19 main protease, pharmacophore field templates were generated for the FDA approved SARS-CoV-2 repurposed drugs comprising Nafamostat, Hydroxyprogesterone caporate and Camostat mesylate. These drugs after field pharmacophore generation were now bioactive conformations which help in the identification of common pharmacophores features of marine drugs [51]. Fig. 2 showed the negative field points in cyan color which generated due to the interactions of positive regions or H-bond donors of receptor target with molecule. While positive field points are represented by red color which generated due to the interaction of acceptor atoms or negative region of target receptor with molecule atoms. Gold color indicates the

Table 2
The LF VS and ΔG score along with the interacting active residues of COVID-19 main protease co-crystal receptor site

Target protein PDB ID	Compounds		LF VS score virtual screening score kcal/Mol	LF ΔG docking score kcal/Mol	H-bonded interacting residues
7LYI	Active marine drugs	Trabectedin	−12.68	−11.55	GLU 166
		Holichondrin B	−15.7	−9.70	LEU 282 PHE 3 THR 199 TRP 207
		Didemnin B	−9.72	−7.10	LEU 287 LEU 287 GLU 290
		Bretuximab	−10.26	−8.89	THR 26 HIS 163
		Lestaurtinib	−9.72	−7.64	THR 190
		Bryostatin	−11.29	−8.78	GLN 192, GLU 166, GLY 143
		Apilidin	−10.69	−8.60	ASP 197
		Marizomib	−10.39	−7.52	GLU 166, GLU 166
	Standard drugs	Nafamostat	−9.31	−7.97	THR 26
		Camostat mesylate	−9.48	−8.20	THR 26 THR 190
		Hydroxyprogesterone caproate	−9.70	−9.09	No interaction
7L0D	Active marine drugs	Trabectedin	−10.13	−9.38	ARG 188, ASN 142, GLY 143
		Holichondrin B	−12.80	−8.62	TRP 207 LEU 282 LYS 5
		Didemnin B	−10.02	−7.70	ALA 285 GLY 166
		Bretuximab	−10.26	−9.30	HIS 163 GLY 143
		Lestaurtinib	−11.91	−8.93	LEU 287
		Bryostatin	−12.16	−8.07	GLY 195, ASP 197, LYS 137
		Apilidin	−9.50	−8.05	No interaction
		Marizomib	−11.18	−8.02	HIS 164
	Standard drugs	Nafamostat	−8.45	−6.95	THR 304 ASP 295
		Camostat mesylate	−9.71	−8.19	ASN 142 TYR 54
		Hydroxyprogesterone caproate	−10.16	−9.53	GLY 143
7JQ2	Active marine drugs	Trabectedin	−10.64	−9.94	GLU 166, LYS 97
		Holichondrin B	−13.13	−8.29	GLY 138 GLU 166
		Didemnin B	−12.23	−9.60	GLU 166 GLU 166
		Bretuximab	−10.42	−9.35	ASN 142 HIS 163
		Lestaurtinib	−8.35	−7.13	GLN 299
		Bryostatin	−12.01	−9.72	GLY 143, HIS 163
		Apilidin	−10.41	−8.69	ALA 7
		Marizomib	−11.47	−8.30	HIS 164, ASN 142
	Standard drugs	Nafamostat	−9.44	−7.92	PHE 140 TYR 54 MET 49
		Camostat mesylate	−10.50	−8.97	ASN 142 MET 165 MET 49 TYR 54
		Hydroxyprogesterone caproate	−9.05	−8.33	No interaction
7CA8	Active marine drugs	Trabectedin	−11.55	−9.95	GLY 11, LYS 97
		Holichondrin B	−13.46	−7.89	ARG 105 ASN 151 THR 111 ARG 298
		Didemnin B	−11.87	−9.42	THR 111 GLN 110 ARG 105
		Bretuximab	−9.43	−8.12	GLN 127
		Lestaurtinib	−9.16	−6.01	THR 190, GLU 166,
		Bryostatin	−11.05	−8.37	PHE 181, ARG 105
		Apilidin	−9.79	−8.13	ARG 105 PHE 181

(*continued on next page*)

Table 2 (*continued*)

Target protein PDB ID	Compounds		LF VS score virtual screening score kcal/Mol	LF ΔG docking score kcal/Mol	H-bonded interacting residues
		Marizomib	−10.86	−7.68	LYS 5, ARG 4
	Standard drugs	Nafamostat	−8.91	−7.39	ASP 155
		Camostat mesylate	−9.23	−7.62	ASP 155 TYR 154 ASP 155
		Hydroxyprogesterone caproate	−9.83	−9.04	ASN 142 TYR 154
7BQY	Active marine drugs	Trabectedin	−10.54	−9.31	GLN 110, TYR 154
		Holichondrin B	−13.79	−7.99	ASP 295 PHE 294
		Didemnin B	−9.18	−7.34	LYS 5 PHE 3
		Bretuximab	−8.76	−7.87	ASP 289
		Lestaurtinib	−8.90	−6.55	THR 111
		Bryostatin	−12.02	−9.68	ASP 153, SER 158
		Apilidin	−9.77	−7.32	LYS 102 TYR 154
		Marizomib	−6.94	−6.46	LYS 5, LYS 135
	Standard drugs	Nafamostat	−7.31	−5.42	LYS 12
		Camostat mesylate	−9.28	−7.77	GLN 127
		Hydroxyprogesterone caproate	−9.26	−8.53	THR 111
7BUY	Active marine drugs	Trabectedin	−11.45	−10.38	GLU 166, THR 25, HIS 41
		Holichondrin B	−12.17	−7.01	LEU 50 GLY 143
		Didemnin B	−11.36	−7.54	ASN 142 CYS 44
		Bretuximab	−8.80	−7.80	No interaction
		Lestaurtinib	−11.68	−7.16	CYS 44, ASN 142
		Bryostatin	−10.61	−8.18	THR 25, GLN 189
		Apilidin	−9.86	−8.33	GLN 189 THR 190
		Marizomib	−7.40	−7.05	HIS 164
	Standard drugs	Nafamostat	−7.31	−5.58	PRO 168
		Camostat mesylate	−8.21	−6.98	GLN 189 GLU 166 THR 26
		Hydroxyprogesterone caproate	−8.37	−7.72	THR 26

hydrophobic points, these regions have high polarizability and yellow color field points generated are for Van der Waals interactions. These field points generated and these aligned reference molecules help in generating the conformation hunt and alignment of marine molecules [46–50].

3.1.2. 3D-QSAR and activity atlas model development and their statistical analysis

In order to generate 3D-QSAR model building, chemical descriptors derived from reference molecules Field point template model used in the alignment of 49 marine data sets. Field based 3D-QSAR model was built by using PLS regression analysis. Of the 49 marine compounds in data set 36 compounds were selected for training set and remaining were categorized as test set molecules. Leave one out cross-validation type was used for models containing small number of training sets. PLS regression analysis was predicted by analyzing twenty components which showed one component as lead for the model. [45,56].

3.1.3. Validation of 3D-QSAR model

3D-QSAR model (Fig. 3) was affirmed by various statistical tests including correlation coefficient R^2 which showed the descriptive accuracy of model to be 83.3 % ($r^2 = 0.833$) as it narrated the importance of regression model, regression co-efficient Q^2 which depict the predicted activity accuracy of model to be 60.01 % ($q^2 = 0.601$). These values which are more than 50 % confirmed the robustness of model for predicting the virtual high throughput screening (vHTS) of marine drugs for SARS-CoV-2 drug repurposing. While RMS error value was 42.62 % (RMSE = 0.4262), which validated the strength of model (Figs. 4 & 5) [55,57,58].

3.1.4. Exploration of field points for inhibiting SARS-CoV-2 main protease

Flare 3D-QSAR ligand-based screening provide the three-dimensional view of field-based properties on which model was constructed. Co-efficient of variance of training set was explored in three-dimensional format by 3D view GUI. These field-based properties have considerable impact on the biological potentials of marine drugs. Bigger field points correlated to more enhanced binding affinity values. To comprehend the field points in 3D view, reference drug was superposed to these points. Results showed the more negative cyan color field points means presence of more electron withdrawing groups enhance the biological potential of molecules. Presence of big green filed points confirmed the positive steric filed points (Fig. 6). High variance points suggest the structural changes in molecules and lower field points suggest the no changes necessary for enhanced biological potential [7,55,57,58].

3.1.5. Activity maximum and minimum from average of actives models

By following these algorithmic values compounds were categorized into active and inactive compounds. This model of activity atlas depicts the average shape, electrostatic and hydrophobic potential areas which all the molecules in dataset have in common with respect to reference drugs. On the basis of average active model, compounds with pIC_{50} activity score of more than 8.22 were categorize as fully active compounds while remaining compounds were inactive. This model (Fig. 7) visualizes the high or beneficial activity areas in molecules which reference drug and active molecules share in common. Total (9) nine

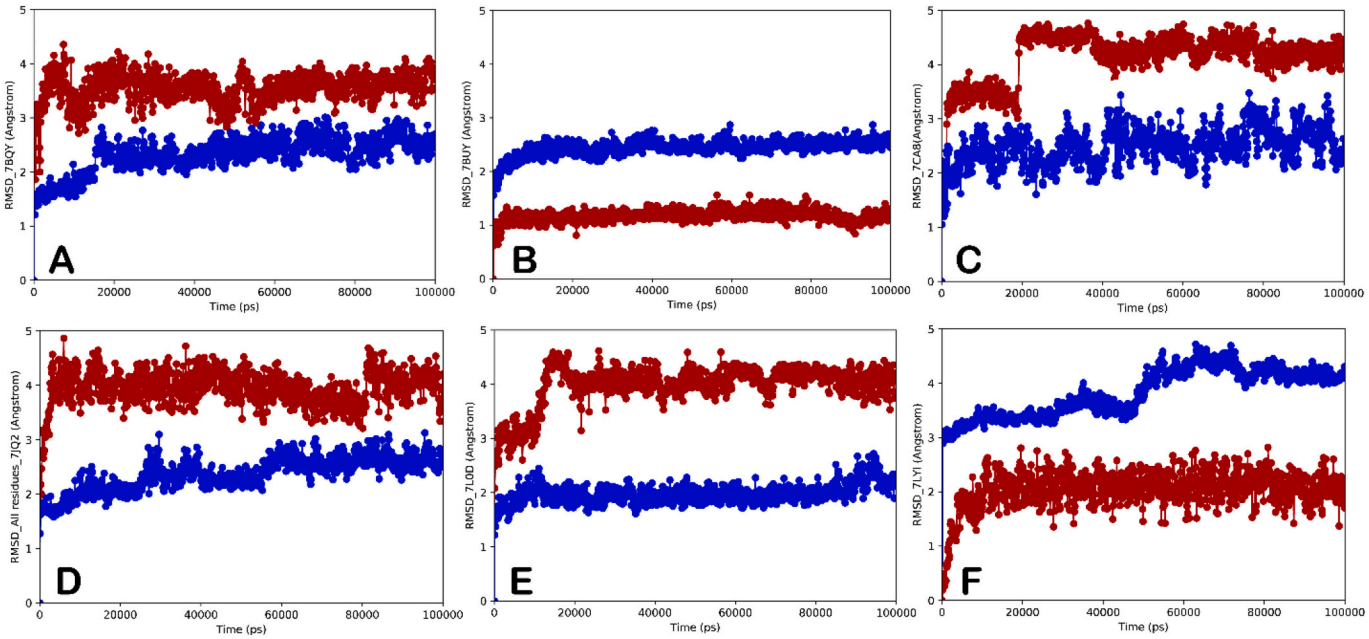

Fig. 11. (A) RMSD regarding the complex main protease (blue line) and Holichondrin B (red line) considering the PDB 7BQY; (B) RMSD regarding the complex main protease (blue line) and Holichondrin B (red line) considering the PDB 7BUY; (C) RMSD regarding the complex main protease (blue line) and Holichondrin B (red line) considering the PDB 7CA8; (D) RMSD regarding the complex main protease (blue line) and Holichondrin B (red line) considering the PDB 7JQ2; (E) RMSD regarding the complex main protease (blue line) and Holichondrin B (red line) considering the PDB 7L0D; (F) RMSD regarding the complex main protease (blue line) and Holichondrin B (red line) considering the PDB 7LYI. Pictures were generated by Simulation Event Analysis available in Desmond. (For interpretation of the references to color in this figure legend, the reader is referred to the web version of this article.)

compounds shown in Fig. 7 and Table 1 falls into the criterion of active compounds [7,57,58].

3.1.6. *Activity cliff summary*

Activity cliff summary of molecules highlights the structure activity relationship (SAR) of active molecules in comparison with SARS-Covid-19 repurposed drugs, shown in Fig. 8. These summary diagrams correlate the active parts of marine drugs with reference drug. Maximum matching suggests the highest similarity with SARS-CoV-2 drugs. Hydrophobic activity cliff summary of active molecules is visualized into two colors green and magenta, area covering in green color could make more hydrophobic interactions while magenta color covered area was unfavorable. In the same way shape cliff summary revealed the favorable steric bulk areas in green color and unfavorable areas in magenta color [7,58].

3.1.7. *Regions explored in activity atlas (AA) model*

Third feature of AA model explored the descriptive features of a molecule regardless of its biological activities. Fig. 9 shows that this feature cover the common regions of active molecules in comparison to reference drugs for SARS-CoV-2. Electropositive, electronegative and hydrophobicity surface contour of active molecules provide strong evidence for drug repurposing of these eleven molecules as repurposed drug for treating SARS-CoV-2. As more positive and negative region i.e., presence of red and cyan surface contour around the active atoms is an indication of strong SAR with the SARS-CoV-2 repurposed reference drugs. Average regions explored also revealed the inactive regions within active molecules which would not take any part in suppressing the SARS-CoV-2 viral activities [7,58].

3.2. *Molecular docking*

The docking studies were carried out to check the binding pattern of active nine compounds and to revealed the binding affinity values for the active receptor site of COVID-19 main protease co-crystal structure and active nine compounds of marine dataset. Docking studies were carried out on the compounds obtained after ligand-based drug design approach. In Flare, normal docking demonstrated various docking poses, configuration and orientations. Hydrogen bonding, Van der Waals interactions, pi-alkyl and alkyl interactions were involved in defining the binding affinity values for the active compounds.

Fig. 10 (a-e) showed the best pose of active nine compounds obtained from ligand-based drug designing approach. For hit to lead identification of compounds based on structure-based drug designing, these nine (9) active compounds were docked against COVID-19 main protease co-crystal structures. Molecular docking results predicted the good virtual screening score labelled as LF VS score and molecular docking score labelled as LF ΔG in comparison to standard drugs used. Table 2 showed the LF VS and ΔG score along with the interacting active residues of COVID-19 main protease co-crystal receptor site. Fig. 10 showed the binding pattern of active compounds into the binding cavity of receptor active site along with standard drugs. Detailed molecular analysis depicted that Halichondrin B showed the high binding affinity score with co-crystal structures of COVID-19 main protease. Thus, in silico study characterize Holichondrin B as lead inhibitor in comparison to standard drugs for SARS-CoV-2 inhibition [55,58–60].

3.3. *Molecular dynamics*

In order to establish the most likely binding site for the selected compound, we have performed a series of MD simulation experiments on all the complexes generated by docking studies. This investigation allowed us to establish the binding stability of Holichondrin B in diverse possible binding sites found on SARS-CoV-2 main protease using the molecular docking approach. Accordingly, after 100 ns of MD simulation in explicit solvent, we evaluated the RMSD to assess the stability of the selected complexes and in particular for evaluating whether the ligand was able to maintain a strong interaction within the binding sites. The output of this calculation is reported in Fig. 11A-F.

Based on MD calculations, some of the identified binding sites by

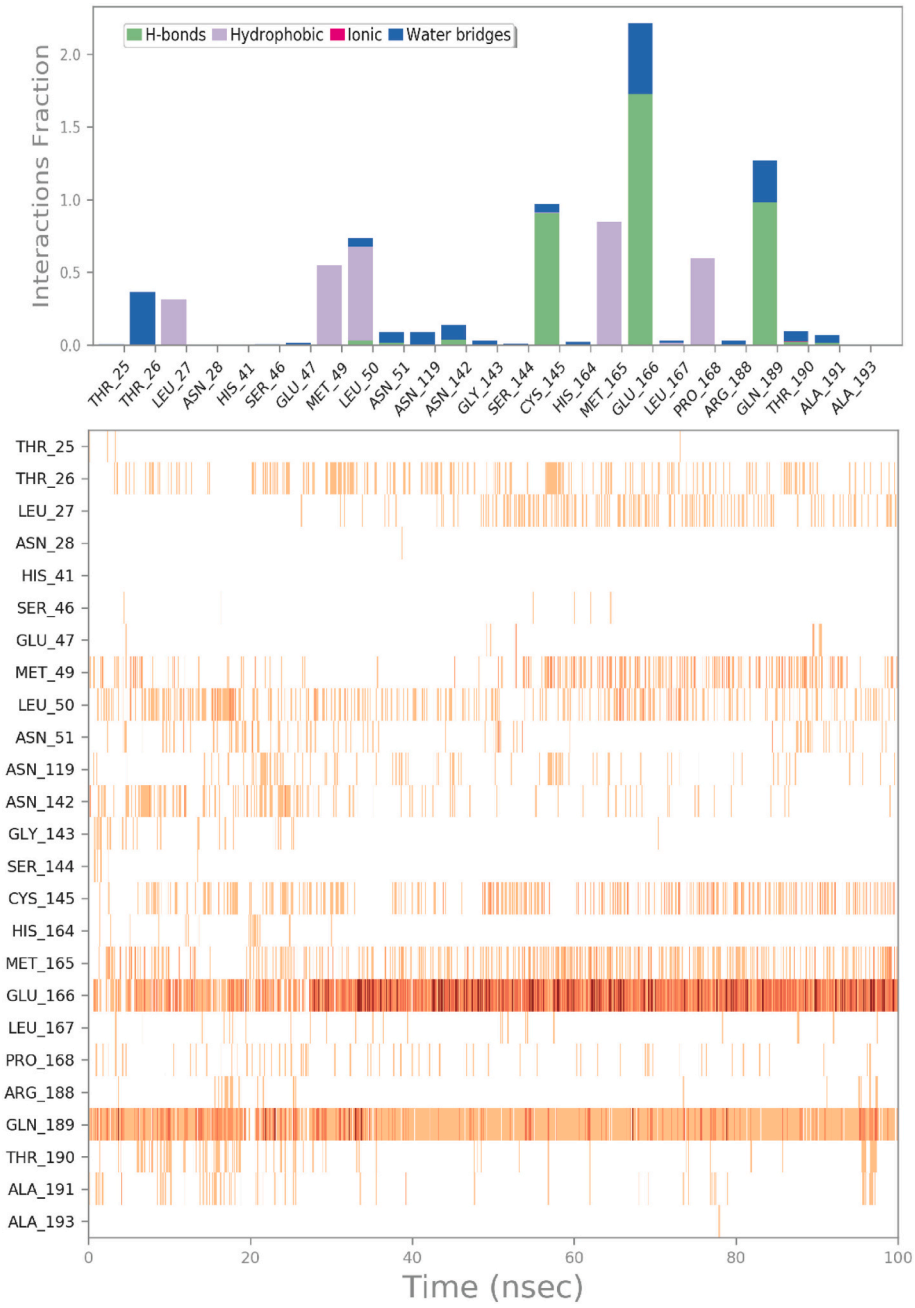

Fig. 12. Holichondrin B monitored in the course of the MD run. The interactions can be grouped into four types: H-bonds (green), hydrophobic (grey), ionic (magenta), and water bridges (blue). The subsequent diagram of the figure illustrates a timeline description of the main interactions. A darker hue of orange indicates that some residues make many distinct contacts with the ligand. (For interpretation of the references to color in this figure legend, the reader is referred to the web version of this article.)

molecular docking were not potentially suitable to host the Holichondrin B, while one of them, due to the stability of the complex and the interactions maintained, could represent a possible binding site for Holichondrin B for interacting with SARS-CoV-2 main protease. In particular, the complex derived from docking calculations using the SARS-CoV-2 main protease crystal structure with PDB code 7BQY (Fig. 11A) did not show satisfactory stability and the compound lacked the interaction with the retrieved binding site showing a very large RMSD, indicating frequent conformational changes with no stable model of interaction. Consequently, due to the large RMSD of Holichondrin B, linked to poor stability of the complex (Fig. 11A, blue line), this site is deprioritized from further analysis. A similar trend was observed for the other complexes derived from docking calculations using the SARS-CoV-2 main protease crystal structure with PDB codes 7CA8 (Fig. 11C), 7JQ2 (Fig. 11D), 7L0D (Fig. 11E), and 7LYI (Fig. 11F). In all these simulations, we observed a limited interaction of Holichondrin B within the selected binding sites, lacking relevant contacts with several conformational changes of the ligand and a poor stability of the protein complexes as indicated by the large RMSD value. On the contrary, as reported in Fig. 11B, the complex derived from docking calculation using the SARS-CoV-2 main protease crystal structure with PDB code 7BUY showed very strong stability and the model of interaction regarding Holichondrin B within the binding site of SARS-CoV-2 main protease is very stable, showing a smaller RMSD with respect to the other generated complexes. Due to the results, we performed further analysis on this binding site as reported below. Interestingly, this binding site is the canonical binding site for main protease inhibitors in which there is the catalytic center represented by Cys145. In order to gain further insight into the potential mechanism of action of Holichondrin B within the selected binding site, we performed a timeline interaction model analysis, derived from MD simulation, for providing a more comprehensive result. As reported in Fig. 12,

Holichondrin B could be able to target specific residues in the well-established binding site, forming polar contacts with key residues for the protease activity. In particular, Holichondrin B can strongly interact with Cys145 at the S1' subsite and with Glu166 at the S1 subsite. Furthermore, we observed strong interactions with the residues Met165 and Pro168 at the S4 subsite. Finally, Holichondrin B could be also able to target residues at the S2 subsite (Thr25, Thr26, and sporadically His41), and at the S3 subsite (Met49, Leu50, Gln189, and marginally Thr190).

According to the performed analysis, Holichondrin B could be able to target relevant residues involved in the activity of SARS-CoV-2 main protease, and due to the good stability of the complex linked to insignificant conformational changes of the ligand, the identified binding site, corresponding to the orthosteric binding site of the main protease, can be the more suitable for Holichondrin B to interact with SARS-CoV-2 main protease.

4. Conclusions and future perspective

Artificial intelligence (AI) and machine learning (ML) tools have revolutionized the drug discovery industry and research. Development of vaccine for COVID-19 was also the result of these ML tools. However, with the increasing population and increasing positive cases along with high rates of death due to SARS-CoV-2 and incomplete distribution of vaccine throughout the world has urge the scientists to repurposed the FDA approved drugs for prevention and cure of COVID-19 symptoms.

In this work, we reported the most novelist and cutting edge computer aided techniques for drug repurposing. FDA approved marine drugs database was retrieved from billions of large chemical libraries and ligand based AI drug discovery tools i.e., 3D-QSAR and activity Atlas models was generated. Best active compounds were employed to structure based drug discovery tools in which protein receptor target was also taken into consideration. AI and ML both proven to be efficient tools in drug repurposing for COVID-19, as out of 49 drugs which were screened by ligand and structure based drug designing only one compound fulfill the criterion of lead drug which is Holichondrin B.

Conclusively, this lead compound has great potential to be transformed to clinical trials thus providing an alternative to vaccine therapy specially for cancer patients having SARS-CoV-2 symptoms.

Declaration of competing interest

There is no conflict of interest.

Data availability

All data generated or analyzed during this study are included and available as its supplementary information files.

Acknowledgements

Authors are thankful to Pakistan science Foundation and Higher Education Commission of Pakistan to provide to support study.

CRediT authorship contribution statement

Naila Attiq[1] = Library preparation, Drafting, Molecular Docking; **Uzma Arshad**[1]: 3D-QSAR, Activity measurement, pharmacophore generation; **Simone Brogi**[2] = MD Simulation; **Nusrat Shafiq**[1]*: conceptualization, supervision, Molecular docking study, Funding; **Fazeelat Imtiaz**[1]: proof reading, English check, Figure quality and resolution; **Maryam Rashid**[1]: Drafting, evaluation of results; **Shagufta Parveen**[1]: data analysis, Literature; **Nadia Noor** = over all editing, checking.

Appendix A. Supplementary data

Supplementary data to this article can be found online at https://doi.org/10.1016/j.ijbiomac.2022.09.086.

References

[1] J. Xu, L. Gao, H. Liang, S.-D. Chen, In silico screening of potential anti–COVID-19 bioactive natural constituents from food sources by molecular docking, Nutrition 82 (2021), 111049.
[2] J. Liu, X. Zheng, Q. Tong, W. Li, B. Wang, K. Sutter, M. Trilling, M. Lu, U. Dittmer, D. Yang, Overlapping and discrete aspects of the pathology and pathogenesis of the emerging human pathogenic coronaviruses SARS-CoV, MERS-CoV, and 2019-nCoV, J. Med. Virol. 92 (5) (2020) 491–494.
[3] G. Pascarella, A. Strumia, C. Piliego, F. Bruno, R.D. Buono, F. Costa, S. Scarlata, F. E. Agrò, COVID-19 diagnosis and management: a comprehensive review, J. Intern. Med. 288 (2) (2020) 192–206.
[4] I.A. Guedes, L.S. Costa, K.B. Dos Santos, A.L. Karl, G.K. Rocha, I.M. Teixeira, M. M. Galheigo, V. Medeiros, E. Krempser, F.L. Custódio, Drug design and repurposing with DockThor-VS web server focusing on SARS-CoV-2 therapeutic targets and their non-synonym variants, Sci. Rep. 11 (1) (2021) 1–20.
[5] F. Yan, F. Gao, An overview of potential inhibitors targeting non-structural proteins 3 (PLpro and Mac1) and 5 (3CLpro/Mpro) of SARS-CoV-2, Comput. Struct. Biotechnol. J. 19 (2021) 4868.
[6] Y. Wu, W. Ho, Y. Huang, D.-Y. Jin, S. Li, S.-L. Liu, X. Liu, J. Qiu, Y. Sang, Q. Wang, SARS-CoV-2 is an appropriate name for the new coronavirus, Lancet 395 (10228) (2020) 949–950.
[7] P. Kalhotra, V.C. Chittepu, G. Osorio-Revilla, T. Gallardo-Velazquez, Field-template, QSAR, ensemble molecular docking, and 3D-RISM solvation studies expose potential of FDA-approved marine drugs as SARS-CoVID-2 Main protease inhibitors, Molecules 26 (4) (2021) 936.
[8] K. Li, S. Maja, S. Gorana, B. Ilić, P. Milan, M. Lu, P. Branislav, Đ.M. Ivana, Š. Marina, Č. Valentina, Insight into diversity of bacteria belonging to the order rickettsiales in 9 arthropods species collected in Serbia, Sci. Rep. 9 (18680) (2019) 1–16.
[9] S. Kannan, P.S.S. Ali, A. Sheeza, K. Hemalatha, COVID-19 (Novel coronavirus 2019)-recent trends, Eur. Rev. Med. Pharmacol. Sci. 24 (4) (2020) 2006–2011.
[10] S. Khan, R. Siddique, M.A. Shereen, A. Ali, J. Liu, Q. Bai, N. Bashir, M. Xue, Emergence of a novel coronavirus, severe acute respiratory syndrome coronavirus 2: biology and therapeutic options, J. Clin. Microbiol. 58 (5) (2020) e00187-20.
[11] I. Khater, A. Nassar, In silico molecular docking analysis for repurposing approved antiviral drugs against SARS-CoV-2 main protease, Biochem. Biophys. Rep. (2021), 101032.
[12] D. Worldometer, COVID-19 coronavirus pandemic, World Health Organization, 2020. www.worldometers.info.
[13] J. Helms, S. Kremer, H. Merdji, R. Clere-Jehl, M. Schenck, C. Kummerlen, O. Collange, C. Boulay, S. Fafi-Kremer, M. Ohana, Neurologic features in severe SARS-CoV-2 infection, N. Engl. J. Med. 382 (23) (2020) 2268–2270.
[14] X. Huang, F. Wei, L. Hu, L. Wen, K. Chen, Epidemiology and clinical characteristics of COVID-19, Arch. Iran. Med. 23 (4) (2020) 268–271.
[15] P. Sun, X. Lu, C. Xu, W. Sun, B. Pan, Understanding of COVID-19 based on current evidence, J. Med. Virol. 92 (6) (2020) 548–551.
[16] A. Zumla, J.F. Chan, E.I. Azhar, D.S. Hui, K.-Y. Yuen, Coronaviruses—drug discovery and therapeutic options, Nat. Rev. Drug Discov. 15 (5) (2016) 327–347.
[17] A.B. Durojaiye, J.-R.D. Clarke, G.A. Stamatiades, C. Wang, Repurposing cefuroxime for treatment of COVID-19: a scoping review of in silico studies, J. Biomol. Struct. Dyn. (2020) 1–8.
[18] A. Mittal, K. Manjunath, R.K. Ranjan, S. Kaushik, S. Kumar, V. Verma, COVID-19 pandemic: insights into structure, function, and hACE2 receptor recognition by SARS-CoV-2, PLoS Pathog. 16 (8) (2020), e1008762.
[19] L. Mousavizadeh, S. Ghasemi, Genotype and phenotype of COVID-19: their roles in pathogenesis, J. Microbiol. Immunol. Infect. 54 (2) (2021) 159–163.
[20] J. Lan, J. Ge, J. Yu, S. Shan, H. Zhou, S. Fan, Q. Zhang, X. Shi, Q. Wang, L. Zhang, Structure of the SARS-CoV-2 spike receptor-binding domain bound to the ACE2 receptor, Nature 581 (7807) (2020) 215–220.
[21] H. Vennema, G.J. Godeke, J. Rossen, W.F. Voorhout, M.C. Horzinek, D. Opstelten, P. Rottier, Nucleocapsid-independent assembly of coronavirus-like particles by co-expression of viral envelope protein genes, EMBO J. 15 (8) (1996) 2020–2028.
[22] Y. Siu, K. Teoh, J. Lo, C. Chan, F. Kien, N. Escriou, S. Tsao, J. Nicholls, R. Altmeyer, J. Peiris, The M, E, and N structural proteins of the severe acute respiratory syndrome coronavirus are required for efficient assembly, trafficking, and release of virus-like particles, J. Virol. 82 (22) (2008) 11318–11330.
[23] J.F.-W. Chan, K.-H. Kok, Z. Zhu, H. Chu, K.K.-W. To, S. Yuan, K.-Y. Yuen, Genomic characterization of the 2019 novel human-pathogenic coronavirus isolated from a patient with atypical pneumonia after visiting Wuhan, Emerg. Microbes Infect. 9 (1) (2020) 221–236.
[24] S. Mazzini, L. Musso, S. Dallavalle, R. Artali, Putative SARS-CoV-2 mpro inhibitors from an in-house library of natural and nature-inspired products: a virtual screening and molecular docking study, Molecules 25 (16) (2020) 3745.
[25] J. Shang, Y. Wan, C. Luo, G. Ye, Q. Geng, A. Auerbach, F. Li, Cell entry mechanisms of SARS-CoV-2, Proc. Natl. Acad. Sci. 117 (21) (2020) 11727–11734.
[26] N.D. Gajjar, T.M. Dhameliya, G.B. Shah, In search of RdRp and mpro inhibitors against SARS CoV-2: molecular docking, molecular dynamic simulations and ADMET analysis, J. Mol. Struct. 1239 (2021), 130488.

[27] Z. Haider, M.M. Subhani, M.A. Farooq, M. Ishaq, M. Khalid, R.S.A. Khan, A. K. Niazi, In Silico Discovery of Novel Inhibitors Against Main Protease (Mpro) of SARS-CoV-2 Using Pharmacophore and Molecular Docking Based Virtual Screening From ZINC Database, Preprint, 2020.
[28] U. Qamar, M. Tahir, S.M. Alqahtani, M.A. Alamri, L.-L. Chen, Structural basis of SARS-CoV-2 3CLpro and anti-COVID-19 drug discovery from medicinal plants, Chin. J. Pharm. Anal. 10 (4) (2020) 313–319.
[29] Z. Jin, X. Du, Y. Xu, Y. Deng, M. Liu, Y. Zhao, B. Zhang, X. Li, L. Zhang, C. Peng, Structure of M pro from SARS-CoV-2 and discovery of its inhibitors, Nature 582 (7811) (2020) 289–293.
[30] S. Gupta, A.K. Singh, P.P. Kushwaha, K.S. Prajapati, M. Shuaib, S. Senapati, S. Kumar, Identification of potential natural inhibitors of SARS-CoV2 main protease by molecular docking and simulation studies, J. Biomol. Struct. Dyn. 39 (12) (2021) 4334–4345.
[31] C. Niu, J. Yin, J. Zhang, J.C. Vederas, M.N. James, Molecular docking identifies the binding of 3-chloropyridine moieties specifically to the S1 pocket of SARS-CoV mpro, Bioorg. Med. Chem. 16 (1) (2008) 293–302.
[32] D.W. Kneller, G. Phillips, H.M. O'Neill, R. Jedrzejczak, L. Stols, P. Langan, A. Joachimiak, L. Coates, A. Kovalevsky, Structural plasticity of SARS-CoV-2 3CL M pro active site cavity revealed by room temperature X-ray crystallography, Nat. Commun. 11 (1) (2020) 1–6.
[33] R. Ghosh, A. Chakraborty, A. Biswas, S. Chowdhuri, Evaluation of green tea polyphenols as novel corona virus (SARS CoV-2) main protease (Mpro) inhibitors–an in silico docking and molecular dynamics simulation study, J. Biomol. Struct. Dyn. (2020) 1–13.
[34] K. Świderek, V. Moliner, Revealing the molecular mechanisms of proteolysis of SARS-CoV-2 M pro by QM/MM computational methods, Chem. Sci. 11 (39) (2020) 10626–10630.
[35] Y.L. Ng, C.K. Salim, J.J.H. Chu, Drug repurposing for COVID-19: approaches, challenges and promising candidates, Pharmacol. Ther. 228 (2021), 107930.
[36] H. Malve, Exploring the ocean for new drug developments: marine pharmacology, J. Pharm. Bioallied Sci. 8 (2) (2016) 83–91.
[37] A.M.S. Mayer, K.B. Glaser, C. Cuevas, R.S. Jacobs, W. Kem, R.D. Little, J. M. McIntosh, D.J. Newman, B.C. Potts, D.E. Shuster, The odyssey of marine pharmaceuticals: a current pipeline perspective, Trends Pharmacol. Sci. 31 (6) (2010) 255–265.
[38] V. S, J. RA, Marine drugs: Implication and future studies, Int. J. Pharmacol. 7 (2011) 22–30.
[39] M. A, Marketed marine natural products in the pharmaceutical and cosmeceutical industries: tips for success, Mar. Drugs 12 (2014) 1066–10101.
[40] C. Gm, G. Pg, N. Dj, Impact of natural products on developing new anti-cancer agents, Chem. Rev. 109 (2009) 3012–3043.
[41] A. Martins, H. Vieira, H. Gaspar, S. Santos, Marketed marine natural products in the pharmaceutical and cosmeceutical industries: tips for success, Mar. Drugs 12 (2) (2014) 1066–1101.
[42] A. Mumtaz, U.A. Ashfaq, M.T. ul Qamar, F. Anwar, F. Gulzar, M.A. Ali, N. Saari, M. T. Pervez, MPD3: a useful medicinal plants database for drug designing, Nat. Prod. Res. 31 (11) (2017) 1228–1236.
[43] E. Jacoby, in: ElEmEnts for thE DEvElopmEnt of stratEgiEs for CompounD library EnhanCEmEnt, Small Molecule Medicinal Chemistry: Strategies and Technologies, 2015, p. 13.
[44] O.Prakash Tanwar, C. Karthikeyan, N.S. Hari Narayana Moorthy, P. Trivedi, 3D QSAR of aminophenyl benzamide derivatives as histone deacetylase inhibitors, Med. Chem. 6 (5) (2010) 277–285.
[45] T. Yoshida, S. Hirono, A 3D-QSAR analysis of CDK2 inhibitors using FMO calculations and PLS regression, Chem. Pharm. Bull. 67 (6) (2019) 546–555.
[46] H. Khalilullah, Identification of anti-cancer agents targeting Aldo-Keto Reductase (AKR) 1C3 protein by pharmacophore modeling, virtual screening and molecular docking, ChemistrySelect 6 (45) (2021) 12820–12833.
[47] M. Wagener, J.P. Lommerse, The quest for bioisosteric replacements, J. Chem. Inf. Model. 46 (2) (2006) 677–685.
[48] B.-J. Sung, K. Yeon Hwang, Y. Ho Jeon, J.I. Lee, Y.-S. Heo, J. Hwan Kim, J. Moon, J. Min Yoon, Y.-L. Hyun, E. Kim, Structure of the catalytic domain of human phosphodiesterase 5 with bound drug molecules, Nature 425 (6953) (2003) 98–102.
[49] M. Tu, B.K. Rai, A.M. Mathiowetz, M. Didiuk, J.A. Pfefferkorn, A. Guzman-Perez, J. Benbow, C.R. Guimarães, S. Mente, M.M. Hayward, Exploring aromatic chemical space with NEAT: novel and electronically equivalent aromatic template, J. Chem. Inf. Model. 52 (5) (2012) 1114–1123.
[50] W.R. Pitt, D.M. Parry, B.G. Perry, C.R. Groom, Heteroaromatic rings of the future, J. Med. Chem. 52 (9) (2009) 2952–2963.
[51] P.J. Gane, A. Chan, Molecular fields in ligand discovery, in: Protein-Ligand Interactions, Springer, 2013, pp. 479–499.
[52] G. Floresta, V. Patamia, D. Gentile, F. Molteni, A. Santamato, A. Rescifina, M. Vecchio, Repurposing of FDA-approved drugs for treating iatrogenic botulism: a paired 3D-QSAR/Docking approach, ChemMedChem 15 (2) (2020) 256–262.
[53] J.L. Medina-Franco, A.B. Yongye, J. Pérez-Villanueva, R.A. Houghten, K. Martínez-Mayorga, Activity-difference maps and consensus similarity measure characterize structure-activity relationships, J. Cheminf. 4 (1) (2012), 1-1.
[54] V. Tiwari, Pharmacophore screening, denovo designing, retrosynthetic analysis, and combinatorial synthesis of a novel lead VTRA1. 1 against RecA protein of Acinetobacter baumannii, Chem. Biol. Drug Des. 99 (2022) 839–856, https://doi.org/10.1111/cbdd.14037. In this issue.
[55] S. Alam, F. Khan, QSAR and docking studies on xanthone derivatives for anticancer activity targeting DNA topoisomerase IIα, Drug Des. Devel. Ther. 8 (2014) 183.
[56] K. Hasegawa, K. Funatsu, Partial least squares modeling and genetic algorithm optimization in quantitative structure-activity relationships, SAR QSAR Environ. Res. 11 (3–4) (2000) 189–209.
[57] S. Alam, F. Khan, 3D-QSAR studies on maslinic acid analogs for anticancer activity against breast cancer cell line MCF-7, Sci. Rep. 7 (1) (2017) 1–13.
[58] S. Alam, F. Khan, 3D-QSAR, Docking, ADME/Tox studies on Flavone analogs reveal anticancer activity through Tankyrase inhibition, Sci. Rep. 9 (1) (2019) 1–15.
[59] J. Ziemska, J. Solecka, M. Jarończyk, In silico screening for novel leucine aminopeptidase inhibitors with 3, 4-dihydroisoquinoline scaffold, Molecules 25 (7) (2020) 1753.
[60] M.A. Ibrahim, A.H. Abdelrahman, T.A. Mohamed, M.A. Atia, M.A. Al-Hammady, K. A. Abdeljawaad, E.M. Elkady, M.F. Moustafa, F. Alrumaihi, K.S. Allemailem, In silico mining of terpenes from red-sea invertebrates for sars-COV-2 main protease (Mpro) inhibitors, Molecules 26 (7) (2021) 2082.